Check for updates

Catalytic ketonization of palmitic acid over a series of transition metal oxides supported on zirconia oxide-based catalysts†

S. A. Aleem, [ID] [abc] N. Asikin-Mijan, [ID] [ab] A. S. Hussain, [ID] [c] C. H. Voon, [ID] [c] A. Dolfi, [f] S. Sivasangar [ID] *[aeg] and Y. H. Taufiq-Yap [ID] *[abd]

Modification of a ZrO_2 based catalyst with selected transition metals dopants has shown promising improvement in the catalytic activity of palmitic acid ketonization. Small amounts of metal oxide deposition on the surface of the ZrO_2 catalyst enhances the yield of palmitone (16-hentriacontanone) as the major product with pentadecane as the largest side product. This investigation explores the effects of addition of carefully chosen metal oxides (Fe_2O_3, NiO, MnO_2, CeO_2, CuO, CoO, Cr_2O_3, La_2O_3 and ZnO) as dopants on bulk ZrO_2. The catalysts are prepared via a deposition–precipitation method followed by calcination at 550 °C and characterized by XRD, BET-surface area, TPD-CO_2, TPD-NH_3, FESEM, TEM and XPS. The screening of synthesized catalysts was carried out with 5% catalyst loading onto 15 g of pristine palmitic acid and the reaction carried out at 340 °C for 3 h. Preliminary studies show catalytic activity improvement with addition of dopants in the order of La_2O_3/ZrO_2 < CoO/ZrO_2 < MnO_2/ZrO_2 with the highest palmitic acid conversion of 92% and palmitone yield of 27.7% achieved using 5% MnO_2/ZrO_2 catalyst. Besides, NiO/ZrO_2 exhibits high selectivity exclusively for pentadecane compared to other catalysts with maximum yield of 24.9% and conversion of 64.9% is observed. Therefore, the changes in physicochemical properties of the dopant added ZrO_2 catalysts and their influence in palmitic acid ketonization reaction is discussed in detail.

1. Introduction

Development of sustainable routes to produce bio-based compounds from renewable feedstock is the most relevant strategy to counterbalance the inevitable depletion of fossil resources in the near future. Petroleum based lubricants play a pivotal role in engine functions and the supply of this substance is in huge demand. Therefore, the potential of bio-lubricant development and its application has received wider consideration from researchers. The use of bio-based feedstock to produce fuel and lubricants is currently the most sought after route and the use of heterogeneous catalysts are vital in this process.[1] Transforming the bio based feedstock is regarded as a complex process that requires extensive transformative steps in order to reduce the oxygen content of the bio feed, while keeping the carbon and hydrogen intact.[2]

In Malaysia, palm oil and palm-based bio feed are the main source of feedstock for biofuels (biodiesel, green diesel) and other biochemicals in the oleochemical industry. Malaysia currently accounts for 28% of world palm oil production and 33% of world exports. If taken into account of other oils and fats produced in the country, Malaysia accounts for 9.5% and 19.7% of the world's total production and exports of oils and fats.[3] One of the by-products of palm oil extraction is known as Palm Fatty Acids Distillates (PFAD), which accounts for up to 5% of the raw material inputs and considered as an unwanted processing residue.[4] Palm fatty acid distillates are composed of several types of fatty acids with carbon chain lengths in the range of C_{12}–C_{18} with C_{16} being the largest fraction of above 45%.[5]

The highly paraffinic structure of PFAD is suitable for conversion to paraffinic hydrocarbon products. However, PFAD's high oxygen containing constituents needs to be upgraded into feasible starting material for production of fuel, lubricants or other oleochemical synthesis. One of the catalytic reaction pathway that can be employed in converting these

Catalysis Science and Technology Research Centre (PutraCAT), Faculty of Science, Universiti Putra Malaysia, 43400 UPM Serdang, Selangor, Malaysia. E-mail: taufiq@upm.edu.my; Fax: +603-89466758; Tel: +603-89466809

Department of Chemistry, Faculty of Science, Universiti Putra Malaysia, 43400, UPM Serdang, Selangor, Malaysia

PETRONAS Research Sdn Bhd, Kawasan Institusi Bangi, Kajang, 43000 Selangor, Malaysia

Faculty of Science and Natural Resources, Universiti Malaysia Sabah, 88400, Kota Kinabalu, Sabah, Malaysia

Department of Science & Technology, Faculty of Humanities, Management & Science, Universiti Putra Malaysia Kampus Bintulu, Jalan Nyabau, Peti Surat 396, 97008 Bintulu, Sarawak, Malaysia. E-mail: sivasangar@upm.edu.my; Tel: +6086-855743

PETRONAS Research Turin, Trinità 82, 10026 Santena (Turin), Italy

Institut EkoSains Borneo, Universiti Putra Malaysia Sarawak Campus, Jalan Nyabau, 97008 Bintulu, Sarawak, Malaysia

† Electronic supplementary information (ESI) available. See DOI: 10.1039/d0ra10963k

oxygenated compounds is *via* the ketonization reaction.[6] Ketonization converts the carboxylic acids to form new C–C bonds *via* decarboxylative carbon coupling to yield alkanones, carbon dioxide (CO_2) and water (H_2O):[7]

$$2R_1COOH \rightarrow R_1C(=O)R_1 + CO_2 + H_2O \ (R_1 = alkyl) \quad (1)$$
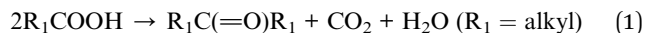
This reaction proves to be an attractive pathway in upgrading bio-derived feedstock in that three oxygen atoms are removed, and the carbon chain is elongated to yield heavier carbon components.[7] The produced alkanones are ready for subsequent process to yield waxes, lubricants and specialty chemicals.[6]

A variety of basic, acidic and amphoteric metal oxide catalysts have been screened in the catalytic ketonization reaction.[8–10] Based on those findings, amphoteric reducible metals such as ZrO_2 have been shown to be a more effective catalyst compared to other oxides in ketonization.[11] Fally *et al.* (2000) reported that high ketonization activity of ZrO_2 catalyst is due to the formation of a highly defective surface, higher Lewis acid content and oxygen vacancies.[12] The role of heterogenous catalysts and the mechanisms of the ketonization reaction have been heavily reviewed in the literature.[9,13] Aranda-Pérez *et al.* (2017) reported 20–60% yield of acetone at low temperature conditions (200–220 °C) over Ru/TiO_2 in hexane diluted acetic acid ketonization.[2] Furthermore, Deng *et al.* (2009) explored the ketonization of aqueous solution of acetic acid using various weak basic metal oxides, finding ceria and manganese supported on silica to have the best conversions of up to 100%.[14] Similarly, propionic acid conversion in 10% N_2 gas stream to pentanone over Mn, Zr, Ce, Th and U on alumina resulted in over 90% yield of ketones whereby these studies mainly focused on short chained carboxylic acids.[10] On the other hand, palm oil ketonization over several metal oxide catalysts at 693 K (Al_2O_3 Puralox SBa 200, MgO–Al_2O_3 Pural MG70, H-ZSM-5 CBV 5524G, and NaX Sylobead MS C544) reported a product composition of predominantly palmitone and pentadecane.[15] Overall, it should be noticed that a variety of feedstock has been used in ketonization, although the focus is mostly on diluted short chained carboxylic acids.

Based on aforementioned literatures, we explore the effect of a series metal oxide dopants (Fe_2O_3, NiO, MnO_2, CeO_2, CuO, CoO, Cr_2O_3, La_2O_3 and ZnO) supported on ZrO_2 for the ketonization of palmitic acid. Therefore, the synergistic effects of these added dopants on ZrO_2 are investigated to convert neat palmitic acid ($C_{15}COOH$) to palmitone ($C_{31}H_{62}O$). Since most of the previous studies focused on ketonization of short chained carboxylic acids (acetic and propionic acid) mostly diluted in solvents, there is a research gap in application of longer chained neat fatty acids as a feedstock for this reaction. Hence, this study aims to illustrate the activity of various metal oxide catalysts in palmitic acid ketonization and identify the most active metal oxide dopants to enhance the product selectivity.

2. Experimental

2.1 Materials

Zinc nitrate hexahydrate (purity 98%, Sigma Aldrich), lanthanum(III) nitrate hydrate (purity 99.9%, Aldrich), cerium(III)

nitrate hydrate (purity 99.5%, Acros Organics), chromium(II) nitrate hydrate (purity > 96%, Riedel deHaen), iron(III) nitrate (purity 98.5%, Bendosen), nickel nitrate hexahydrate (purity 99.5%, Acros Organics), cobalt(II) nitrate hexahydrate (purity > 98%, Systerm), copper(II) nitrate hemipentahydrate (purity > 98.5%, Acros Organics) and zirconium(IV) oxide (ZrO_2) (purity > 98.5% Acros Organics) were obtained. Potassium hydroxide (KOH) at purity > 99% were obtained from Acros Organics. The fatty acid feedstock, palmitic acid was obtained from Acros Organics at purity > 99%. For analysis purposes, internal standard for palmitone (16-hentriacontanone) from Sigma Aldrich is used (GC Grade at purity > 99%) and for dilution, heptane (GC Grade) and chloroform (GC Grade) with purity > 99% from Merck is used. Nitrogen from Air Liquide at purity over >99.9% is used as inert environment for ketonization reactions.

2.2 Catalyst synthesis

Based on previous study done by Hussain *et al.*,[16] the catalyst synthesis method chosen for synthesis of X/ZrO_2 (X: Fe, Cu, Cr, Zn, Ce, Co, Ni, Mn, La) was deposition–precipitation (DP) method. X/ZrO_2 was prepared at room temperature by completely dissolving 5% of metal content (by weight) into 10 mL of deionised water. The metal salt solution was added dropwise into 95 wt% equivalent of zirconium oxide(IV) (ZrO_2) in 20 mL of deionised water. The metal species were further deposited on the ZrO_2 support by adding 0.5 M KOH basic solution (dropwise) until pH 12–13 were reached under vigorous stirring. The final mixture was stirred for 4 h and the solid was separated by filtration, washed with distillate water until pH 7 was reached and dried in an oven at 120 °C under static air condition overnight. The dried solid was then grounded into fine powder and calcined at 550 °C for 2 h.

2.3 Catalyst characterization

The X-ray diffraction (XRD) for powdered catalysts is used to investigate the bulk structure and to determine the crystallographic parameters of the catalysts. The XRD analysis was performed using Shimadzu diffractometer model XRD-6000. The temperature programmed desorption of carbon dioxide (TPD-CO_2) is used to characterize the basic sites of the catalysts using Micromeritics TPD/R/O Autochem 2920 (fully equipped with TCD). The catalyst (~0.05 g) was pre-treated by N_2 gas flow for 30 min and at 250 °C. Then, the catalyst was exposed to CO_2 gas for 1 h at ambient temperature to allow adsorption of CO_2 molecules onto the catalyst surfaces. The excess CO_2 was subsequently flushed out with N_2 gas flow at rate 20 mL min^{-1} for 30 min. The desorption of CO_2 from the basic sites of the catalyst was detected by TCD under helium gas flow (30 mL min^{-1}) from 50 °C to 900 °C and held for 30 min. The surface area and pore properties were calculated by the Brunauer–Emmett–Teller (BET) using Micromeritics ASAP 2020 model. The catalysts were degassed overnight at 150 °C for 8 h to remove moisture and foreign gases adsorbed on the surfaces of the catalyst. Adsorption and desorption process of N_2 on the catalyst surfaces were analysed in a vacuum chamber at 50 °C to 900 °C. Morphological composition of the catalysts were

investigated *via* FESEM images using LEO 1455 VP electron microscope. The FESEM-EDX was performed by Rayny EDX-720 spectrometer for the determination of elemental composition of Mn, O, Zr on the synthesized catalyst. As for elemental composition, X-ray fluorescence (XRF) analysis were performed using Bruker S8 Tiger instrument equipped with a rhodium tube operating at 4 kW. X-Ray photoelectron spectroscopy (XPS) was used to study the chemical states of the modified ZrO_2 catalyst, and the measurement was carried out using a Thermo Scientific (K-Alpha) system.

2.4 Ketonization reaction

The ketonization of palmitic acid were carried out in a three necked round bottomed flask set up with heating mantle as shown in Fig. 1S.† Approximately 15 g (0.07 mol) palmitic acid with 0.75 g (5 wt%) of catalyst were placed in three necked round bottomed flask and thereafter purged with N_2 for 15 min. Subsequently, the acid and catalyst mixture were heated at 10 °C min^{-1} to 340 °C under stirring and continuous N_2 flow. The reaction commenced as soon as the desired temperature is reached and maintained for 3 h. Upon completion of the reaction, the flask was cooled down to room temperature and the catalyst was filtered. The liquid product was collected for further analysis.

2.5 Product analysis

The free fatty acid (FFA) conversion of fatty acid model compound was determined by the following (AOCS 5a-40) standard method as eqn (2), where AV_f and AV_p were assigned for acid value of feedstock and product, respectively.

$$FFA \text{ conversion } (\%) = \frac{AV_f - AV_p}{AV_f} \times 100 \quad (2)$$

The resulting liquid products from the ketonization reaction is suspected to contain a myriad of components ranging from unconverted fatty acids to ketones and other hydrocarbons. GCMS and GCFID were used for product identification and product quantification. Prior to GCFID and GCMS analysis, the product is heated to 70 °C and chloroform is used as the solvent. The liquid product was analysed directly, under 10× dilution by chloroform and directly injected into the gas chromatography mass spectrometry (GCMS) analysis using PerkinElmer (Clarus 500 for GC and Clarus 560 S for MS). The unit is equipped with a non-polar DB-5MS column (30 m × 0.25 mm × 0.1 μm) that uses a split less inlet. Identification of the GCMS spectrum peaks was made using the National Institute of Standards and Testing Library.[17] For GCFID, the liquid product was analysed directly using GCFID (Column MXT-1 Restek) from Agilent Technologies also under 10× dilution by chloroform for quantification.

3. Results and discussion

3.1 Physicochemical properties of catalyst

The crystallinity of the synthesised catalysts *via* DP method was analysed by the X-ray diffraction technique and results are
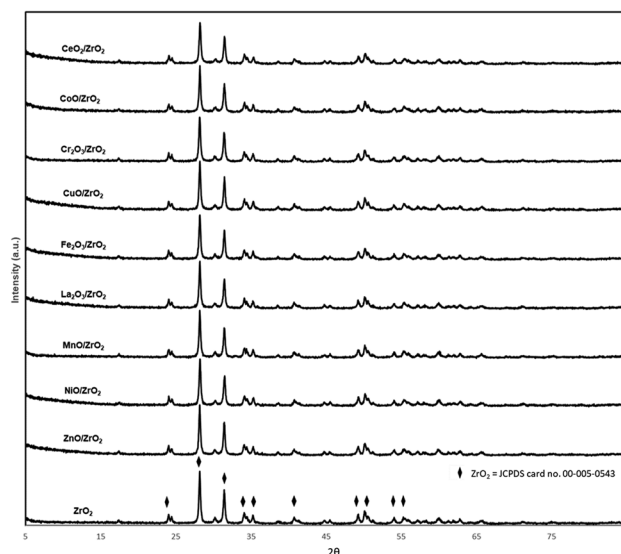

Fig. 1 XRD Diffractogram of ZrO_2 and modified ZrO_2 catalysts.

displayed in Fig. 1. All the catalysts exhibited XRD diffraction peak belonging to monoclinic structure ZrO_2 with crystallite size close to ~37 nm (JCPDS card no. 00-005-0543). Noteworthy to mention that indiscernibility of the peaks of these catalysts is due to the fact the metal oxide dopant content is too low as supported by several studies.[18,19] Notably, no distinctive peaks are seen for ZnO/ZrO_2, CuO/ZrO_2, Cr_2O_3/ZrO_2, CoO/ZrO_2 and CeO_2/ZrO_2 catalysts owing to the fact that all the Zn, Cu, Cr, Co and Ce species most likely highly dispersed on ZrO_2. However, several distinctive single metal oxide peaks belonging to MnO_2 ($2\theta = 88°$; JCPDS card no. 00-001-1206), La_2O_3 ($2\theta = 30°$; JCPDS card no. 00-033-0716) and Ni_2O_3 ($2\theta = 88°$; JCPDS card no. 00-041-0481) were detected for MnO_2/ZrO_2, La_2O_3/ZrO_2 and NiO/ZrO_2 catalysts. Therefore, XRF analysis was used to confirm the presence of added dopants on ZrO_2 catalyst, and the composition are listed in Table 1. The results show a metal dopant composition in the range of 2–4%, confirming the existence of the dopants on the surface of bulk ZrO_2, yet the dopant composition of lower than 5% is mainly due to nature of XRF being a surface analysis that does not represent the average composition of the bulk catalyst.[20] In summary, metal oxide dopant species did not significantly alter the ZrO_2 structure and the existence of distinguishing peaks belonging to specific metal oxides indicates the presence of active metals that is successfully incorporated on ZrO_2.

Table 1 shows the surface area and pore properties of the catalysts tested in this study. The surface area of bulk ZrO_2 (pre-treated similar to dopant added catalysts) is found to be ~6 m^2 g^{-1} with pore diameter around ~24 nm at mesoporous range[21] similar to previous reported studies.[22,23] However, addition of metal dopants slightly improved the surface area of the support (7–17 m^2 g^{-1}) with NiO/ZrO_2 having the highest surface area. This is possibly due to the occurrence of smaller crystallite size after the introduction of NiO into ZrO_2 crystal structure (~34 nm), contributing to the increase in surface area.[24,25] The surface area increment of modified ZrO_2 catalysts is the result of

Table 1 BET surface area, pore properties, XRF and total acidity and basicity of ZrO_2 and modified ZrO_2 catalysts

Catalyst	BET surface area ($m^2 g^{-1}$)	Pore volume ($cm^3 g^{-1}$)	Pore diameter (nm)	Elemental analysis of metal dopant (%)	Crystalline size range (nm)	Total basicity (cm^3 STP g^{-1})	Total acidity (cm^3 STP g^{-1})
ZrO_2	5.60	0.045	23.9	—	38	6.19	4.26
Fe_2O_3/ZrO_2	10	0.055	19.3	3.9	41	5.09	3.73
NiO/ZrO_2	17	0.062	14.0	3.6	34	7.32	5.01
MnO_2/ZrO_2	10	0.064	22.9	3.4	36	7.57	5.76
CeO_2/ZrO_2	11	0.051	19.0	4.2	37	5.20	3.80
CuO/ZrO_2	8	0.049	21.4	3.0	33	8.37	6.38
CoO/ZrO_2	11	0.062	19.1	4.0	38	8.43	6.93
Cr_2O_3/ZrO_2	8	0.047	24.5	1.9	37	3.39	4.53
La_2O_3/ZrO_2	7	0.048	24.5	2.3	39	7.69	6.00
ZnO/ZrO_2	8	0.056	26.7	3.4	37	6.95	3.69

imperfections caused by the added dopant metals to the crystallinity of the catalyst structure hence allowing for more disorder within the catalyst surface, similar to the observations made in previous studies.[26–28] It is postulated that high surface area of the metal oxide catalyst leads to higher number of active sites, facilitating a better catalytic activity for ketonization.[29] Besides, the pore volume of modified ZrO_2 catalysts showed slight increment with highest pore volume observed for MnO_2/ZrO_2 (0.064 $cm^3 g^{-1}$). Pore diameter of the prepared catalysts were found to be similar to ZrO_2 and showed no major
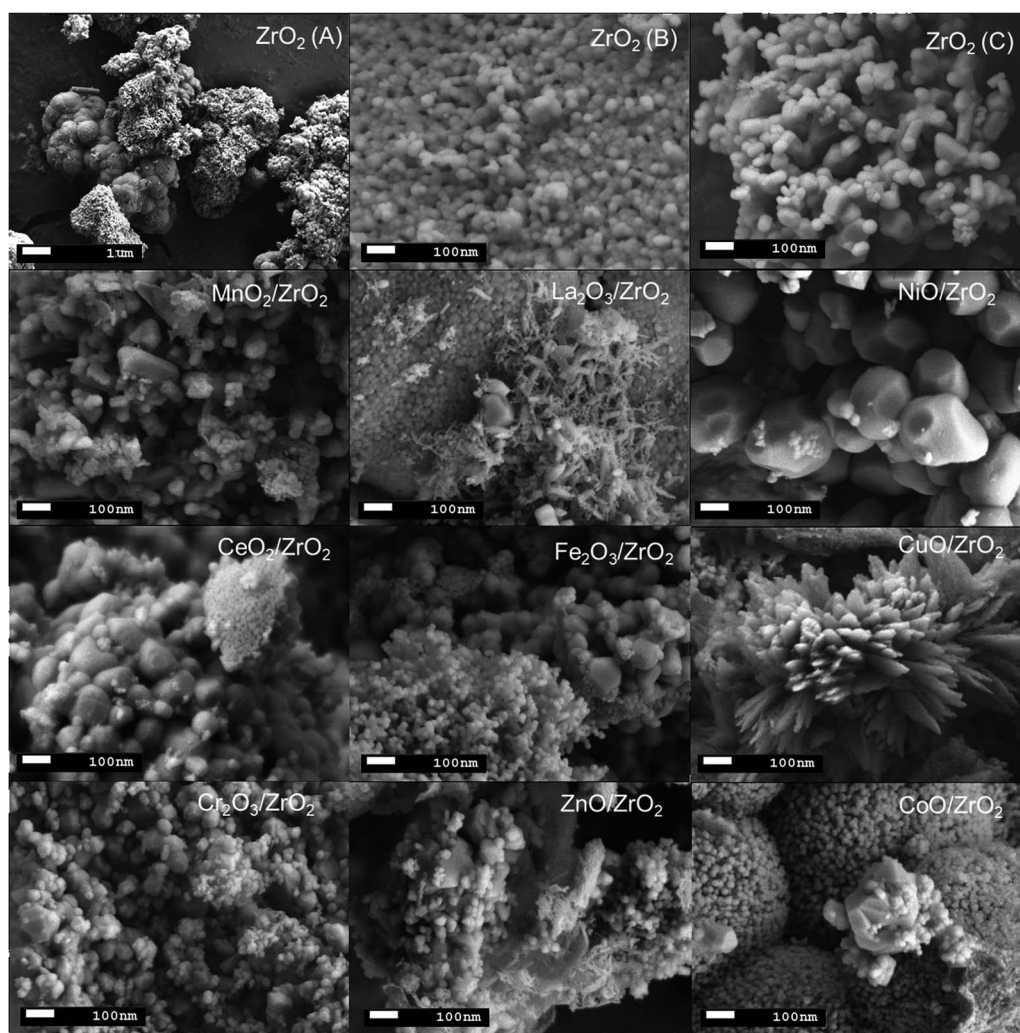
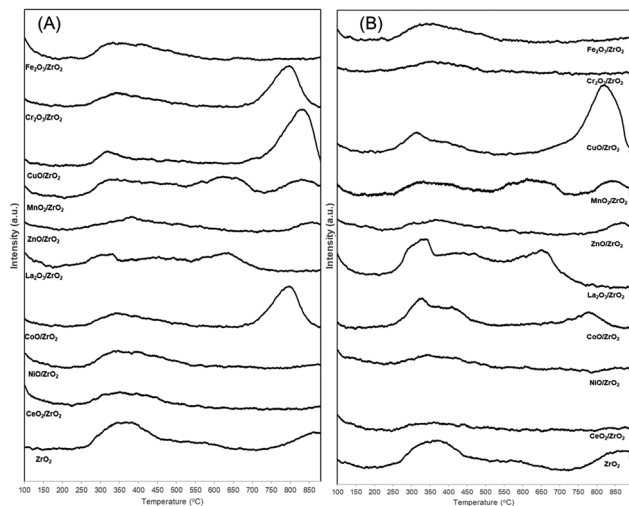Fig. 2 FESEM results of ZrO_2 and modified ZrO_2 catalysts.

Fig. 3 TPD-CO_2 and TPD-NH_3 of ZrO_2 and modified ZrO_2 catalysts.

improvements nor significant differences to that of bulk ZrO_2. In general, these results show that the addition of metal dopants onto ZrO_2 causes only a minor impact to the catalysts' surface area, pore diameter and pore volume.

Surface morphology of all prepared catalysts were carried out using FESEM analysis and the results are displayed in Fig. 2. Bulk ZrO_2 catalyst particles appeared to be a rectangular/cubical-like structure (Fig. 2(A)) while addition of dopants shows some changes in the surface morphology. Particularly, CuO/ZrO_2 appeared to be blade-like structure nanocrystals whereas rest of the catalysts shows similar morphology to bulk ZrO_2 with different size of particle clusters. Hence, observed particles size of the prepared catalysts varies in the range of 76–389 nm with highest and smallest sizes denoted to NiO/ZrO_2 and CoO/ZrO_2 respectively. Based on FESEM results, incorporation of dopants onto ZrO_2 structure resulted notable changes in the particles size, shapes, and metal dispersion on support surface.

Fig. 3(A) represent the TPD-CO_2 profile of the prepared catalyst and the overall basicity is summarized in Table 1. Generally, desorption peaks observed can be divided into three section as weak (<400 °C), moderate (400–550 °C) and strong (>550 °C) basic sites based on the CO_2 desorption temperature.[30,31] Bulk ZrO_2 shows two distinctive peaks at 250–450 °C and >750 °C referred to a sharp weak and broad strong basic site. The presence of weak basic sites in ZrO_2 was found to be more predominant compared to strong site, as reported by Zhang *et al.* (2019).[32] Basic sites in ZrO_2 catalyst refers to the adsorption of CO_2 onto terminal hydroxyl groups and coordinatively unsaturated species such as O^{2-} and Zr^{2+}–O^{2-} interface.[33] Therefore, a series of carbonate species formation occurred on surface area of ZrO_2 which are classified as bicarbonate, monodentate, bidentate and polydentate. Bicarbonate species are the least thermally stable peak which tends to disappear around 373 K while both monodentate and bidentate show moderate thermal stability (573 K) followed by polydentate species that remain adsorbed until 723 K.[34] Modified

ZrO_2 show a significant change in overall basic site density and strength after addition of dopants. Comparatively, incorporation of CoO, CuO and Cr_2O_3 into bulk ZrO_2 resulted a peak at elevated temperatures (<650 °C) attributed to strong basic sites of the catalyst. However, a notable shift in catalyst basicity is observed for CeO_2, NiO, Fe_2O_3 and ZnO added to ZrO_2 at lower temperature region (250–400 °C) ascribed to weak Lewis basic sites. Apart from this, both MnO_2/ZrO_2 and La_2O_3/ZrO_2 catalyst shows a distinctive basicity peak at (500–650 °C) which are considered an intermediate strength basic site formed in between low and high temperature region. Fig. 3(B) on the other hand, represent the TPD-NH_3 profiles of the prepared catalysts and the overall acidity is summarized in Table 1. Similar to TPD-CO_2, the desorption profiles of the catalysts show a distribution of broad peaks in different temperature region suggesting the presence of weak, moderate and strong acid sites.[35] The differences in the strength of these sites are due to the imperfection of the catalyst surface such as oxygen vacancies, corners and kinks[36] and can be also introduced by way of addition of dopants. Bulk ZrO_2 has two distinctive peaks corresponding to weak acid sites and strong acid sites at temperatures (250–400 °C) and (>700 °C) in which the curve agrees with previous studies.[37,38] Addition of dopants have significant effects in the acid site distribution and strength, with the peaks widely differing from the bulk ZrO_2 catalysts. Incorporation of dopants NiO, CeO_2, ZnO, MnO_2, Fe_2O_3 and Cr_2O_3 reduces the intensity of weak acid peak[39–41] while CuO exhibits a notable strong acid peak at elevated temperature region. Interesting to note that both MnO_2/ZrO_2 and La_2O_3/ZrO_2 show a distinctive acidity peak at (500–650 °C) attributed to intermediate strength acidic sites which corroborates with previous studies.[36] It is postulated that catalyst acidity and basicity have a strong influence on the catalytic activity of the ketonization reaction.

3.2 Ketonization and decarboxylation activity of catalysts

Ketonization of palmitic acid was carried out at temperature 340 °C for 3 h with 5 wt% catalyst loading. The preliminary stage catalytic performance is summarised in Table 2. ZrO_2 has a very good balance of acidic and basic characteristic allowing to be behave as an acid–base bifunctional catalyst to facilitate the

Table 2 Performance of catalyst in terms of FA conversion and product yield

Catalyst	Conversion (%)	Palmitone yield (mol%)	Pentadecane yield (mol%)
ZrO_2	84.6	17.1	12.9
Fe_2O_3/ZrO_2	66.7	14.0	15.1
Cr_2O_3/ZrO_2	64.0	17.0	14.7
CuO/ZrO_2	81.3	17.5	14.7
MnO_2/ZrO_2	92.3	27.7	10.8
ZnO/ZrO_2	88.5	11.3	11.8
La_2O_3/ZrO_2	84.3	23.2	13.9
CoO/ZrO_2	92.1	25.1	11.3
NiO/ZrO_2	64.9	3.7	24.9
CeO_2/ZrO_2	93.4	19.8	9.8

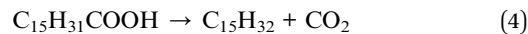adsorption of carboxylate and hydrogen ions.[42] Furthermore, Almutairi *et al.* (2018) and Zaytseva *et al.* (2013) also reported the suitability of ZrO_2 as a catalyst for short chain fatty acids such as acetic acid and valeric acid ketonization reaction that exhibit 80–83% of conversion.[43,44] Similarly, in this investigation, application of long chain fatty acid (palmitic acid) as a feedstock also show high catalytic activity with 85% of conversion achieved using ZrO_2 catalyst. However, incorporation of various dopants onto bulk ZrO_2 catalyst significantly influence the palmitic acid conversion and product selectivity under the fixed reaction conditions. Particularly, MnO_2, CoO and CeO_2 dopants exhibit notable improvement while introduction of NiO, La_2O_3, CuO, ZnO, Cr_2O_3 and Fe_2O_3 shows merely similar or lower catalytic activity than bulk ZrO_2. Precisely, modification of bulk ZrO_2 using MnO_2, CoO, and CeO_2 dopants elevate the overall catalytic activity and palmitic acid conversion was improved to 92–93%. In agreement, Heracleous *et al.* (2017) reported the high catalytic activity of hydrothermally prepared MnO_x catalyst in propanoic acid ketonization reaction that attained conversion above 90%.[45]

The reaction conversion and yield of two major products in the catalytic ketonization of palmitic acid is shown in Table 2. Only the most significant products of the reaction, that includes palmitone (16-hentriacontanone) (C_{31} ketone) and pentadecane ($C_{15}H_{32}$) yields are quantified for catalyst screening. Whereas a wide range of by-products such as alkanes and alkenes of C_9 to C_{13}, tetradecane and tetradecene ($C_{14}H_{30}$ and $C_{14}H_{28}$), heptadecene ($C_{15}H_{30}$), hexadecane ($C_{16}H_{34}$), heptadecanone (C_{17} ketone), mixed range ketone (heavier analogs than C_{17} ketones), as well as trace amounts of aromatics and cycloalkanes are also observed in GCMS spectra (which are not shown). Apart from this, gaseous compounds that includes, CO_2, water vapour and light hydrocarbon gases (C_1–C_4) are formed as a by-product and vented through fume hood. As abovementioned, ketonization is a carbon coupling reaction that combine two carboxyl groups by forming ketone compound *via* elimination of one equivalent water and carbon dioxide molecule.[14,46] However, the occurrence of wide range of product distributions are due to the several other possible reaction mechanisms such as decarboxylation (eqn (4)), decarbonylation (eqn (5)) and thermal cracking (eqn (6)) that might be triggered under palmitic acid ketonization reaction conditions. Regardless of various products, catalytic ketonization of palmitic acid produce palmitone ($C_{31}H_{62}O$) as a major product of reaction as a result of strong dominance of homo-ketonization pathway according to eqn (3). Aside from this, notable amount of pentadecane in the product composition postulates the tendency of decarboxylation route to progress *via* cleavage of carboxyl group from the palmitic acid. This circumstance yields a paraffinic *n*-alkane molecule pentadecane ($C_{15}H_{32}$) with removal of one carbon atom in the form of CO_2 (eqn (4)). Furthermore, small amount of pentadecene (not shown) in the product analysis suggest its formation *via* palmitic acid decabonylation mechanism (eqn (5)). Besides, the possibilities of thermal cracking of palmitic acid according to eqn (6) also arose due to the elevated reaction temperature requirement (>300 °C) for ketonization, rendering the formation of light fractions of (C_9 to C_{13}) and gaseous compounds.[47–49]
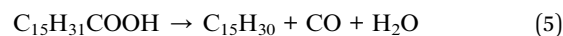
Ketonization:

$$2C_{15}H_{31}COOH \rightarrow C_{31}H_{62}O + CO_2 + H_2O \qquad (3)$$

Decarboxylation:

$$C_{15}H_{31}COOH \rightarrow C_{15}H_{32} + CO_2 \qquad (4)$$

Decarbonylation:

$$C_{15}H_{31}COOH \rightarrow C_{15}H_{30} + CO + H_2O \qquad (5)$$

Thermal cracking:

$$C_{15}H_{31}COOH \rightarrow \text{lighter HC's} + CO_2 + H_2O + CO \qquad (6)$$
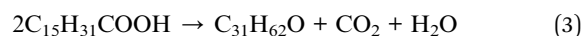
As aforementioned, the performance of the modified ZrO_2 catalyst in palmitic acid ketonization reaction varies due to the alteration in the physico-chemical properties on bulk ZrO_2 caused by added dopants. Therefore, composition of both palmitone and pentadecane yield differ significantly in the range of 3.7–27.7% and 9.8–24.9% respectively with the prepared catalysts. Ketonization under bulk ZrO_2 proceeds with 17.1% of palmitone and 12.9% of pentadecane yield achieved. However, addition of dopants on bulk ZrO_2 significantly influence the yield of both palmitone and pentadecane due to promotional effects of specific catalytic route in palmitic acid conversion. Among the dopants, Ni, Fe, Cr, Cu, Zn, and Ni on ZrO_2 catalyst was found to be ineffective in enhancing palmitone yield and almost similar result (≤17) to bulk ZrO_2 is obtained. Interestingly, reasonable increment in palmitone yield is observed for Mn, La, Co and Ce added ZrO_2 catalyst in the order of bulk ZrO_2 < CeO_2/ZrO_2 < La_2O_3/ZrO_2 < CoO/ZrO_2 < MnO_2/ZrO_2. The combination of La, Co, and Mn dopant on ZrO_2 improves the product selectivity (>23% of ketone yield) whereby highest palmitone yield 27.7% is achieved with MnO_2/ZrO_2 catalyst. Apparently the promotional effects of MnO_2 in propelling ketonization reaction is steadily highlighted in literatures for various short chained fatty acid feedstock.[14,50,51] TEM image of MnO_2/ZrO_2 catalyst (Fig. 2S†) shows that the morphology of the MnO_2/ZrO_2 catalyst consist of elongated crystals which belong to MnO_2 and the pebble like structure belonging to ZrO_2. This corroborates with the findings of Jia *et al.* (2018) where the MnO_2 on ZrO_2 catalyst exhibited long nanofiber structures for MnO_2 and the ZrO_2 exhibited irregular aggregates of nanoparticles.[52] Moreover, the presence of MnO_2 phase in the catalyst was confirmed using XPS analysis. The high-resolution deconvoluted Mn2p spectrum of the MnO_2/ZrO_2 catalyst (Fig. 3S(C)†) consists of two main peaks of the spin–orbit couplet whereby the low binding energy and high binding energy peaks (641.1 eV and 652.2 eV) corresponds to photoelectron states of MnO_2 $2p_{3/2}$ and MnO_2 $2p_{1/2}$.[53,54] It is reported that MnO_x based catalyst exhibit superior catalytic activity with ketone yield reported in the range of 34–90% relative to used feedstock which were generally short chained fatty acids.[55–58] In addition, the reactivity of the carboxylic acids was reported tend to decrease with increasing length of aliphatic chain of acid, which reduces the overall feedstock conversion and reaction efficiency.[50,51] Furthermore, longer chain acids also tend to self-associate into

dimeric pairs through hydrogen bonds that increased their stability than acids in diluted solution.[59] Therefore, the moderate palmitone yield (27.7%) from catalytic palmitic acid ketonization under designated reaction parameters is appropriate considering the long length of the feedstock molecule which is the major limiting factor. Hence, it is apparent that after the preliminary catalyst screening studies, MnO_2/ZrO_2 catalyst was found to be most promising for long chain fatty acid (palmitic acid) ketonization reaction with notable conversion and product selectivity. Sequentially, both La_2O_3/ZrO_2 and CoO/ZrO_2 catalyst also shows adequate performance in palmitic acid ketonization. Both La_2O_3 and CoO was reported highly active in acetic acid ketonization with product selectivity > 96% achieved.[60,61] The performance of the selected catalyst from this study was compared with the other active catalysts in the recent literatures, and the results are listed in Table 3. The MnO_2/ZrO_2 catalyst is shown to be a promising catalyst for ketonization reaction due to its high catalytic activity over undiluted fatty acid application and its comparable ketone yield (27.7%) at moderate reaction temperatures (340 °C).

The role of MnO_x, LaO_x and CeO_x dopants and its catalytic activity is relatively attributed to their modifications of acid and basic sites in the catalyst system.[60,62–64] Correlation of catalyst basicity to ketonization activity is not widely stated in the literature although basicity is often cited as key factor in ketonization reaction mechanisms. However, $TPD-CO_2$ desorption peak positions indicates that the basic site strength of catalysts show some interesting trend for both La_2O_3/ZrO_2 and MnO_2/ZrO_2. The presence of intermediate basic sites peak at temperature range of 450–650 °C shows the unique nature of the catalysts. Albeit, CoO/ZrO_2 doesn't show such obvious peak, we still can observe the shift in weak basic site peak toward intermediate range. Therefore, presence of intermediate basic sites are considered a dominant factor for improving catalytic activity

of ketonization reaction. Moreover, weak basic sites also appeared for CoO and MnO_2 doped ZrO_2 catalysts suggesting cumulative effects of both intermediate and weak basic sites in promoting ketonization reaction. These observation correlates with literature and emphasize the role of catalyst basicity particularly moderate basic sites that reported to be essential in uplifting ketonization activity.[43] Furthermore, it is proposed that CO_2, as the one of the reaction products, has the ability to bind with strong basic sites, rendering them unavailable for ketonization reaction. On the other hand, moderate to weak basic sites which are able to desorb CO_2 at lower temperatures are easily available for the reaction, facilitating ketonization at a more active rate.[43] However, basic sites alone is does not give us adequate information of the effect of active sites on ketonization performance for the catalysts. Previous studies have shown that the existence of acidic sites are applicable in the efficacy of ketonization.[65] The balanced Lewis acid–base pairs due to both acid and basic sites facilitates the abstraction of carboxylate ions onto the catalyst surface in either monodentate or bidentate formation each corresponding to weak or intermediate acid sites.[66] In this study, both La_2O_3/ZrO_2 and MnO_2/ZrO_2 show intermediate acidic peaks as observed in Fig. 3. This finding strongly suggests that the existence of intermediate acid–base sites are vital in enhancing the ketonization reaction performance as reported by Ding *et al.* (2018).[66] Based on all these result, a balance of Lewis acid–base M^{x+}–O^{2-} pairs seem to be a defining characteristic of good ketonization catalyst.[67–70] Apart from this, the impact of catalyst textural properties in palmitic acid ketonization reaction remains unclear. Even though a slight improvement in surface area and porosity occurred with dopant addition, it is not translated into higher catalytic activity or ketone yield. Furthermore, this assumption is strengthened by the previous catalytic conversion of fatty

Table 3 Catalytic activity for acid ketonization on different catalysts

	Catalyst	Feedstock	Reaction time (h)	Reaction temperature (°C)	Catalyst loading (wt%)	Conversion (%)	Ketone product yield (mol%)	Alkane yield (mol%)	Ref.
1	ZrO_2	Neat palmitic acid	3	340	5	84.6	17.1	12.9	This work
2	MnO_2/ZrO_2	Neat palmitic acid	3	340	5	92.3	27.7	10.8	This work
3	MnO_2/ZrO_2	Neat palmitic acid	3	340	15	91.9	30.9	10.5	This work
4	Alumina	Palm oil (~60% palmitic acid)	3	350			18.4^a	11^a	76
5	Al_2O_3 MgO–Al_2O_3 ZSM-5 NaX	Palm oil		420	3		9.8^b 30.2^b 25.3^b 16.1^b	15.6^b 7.4^b 11.4^b 20.3^b	15
6	CeO_2	5% palmitic acid in *p*-xylene	3.3–4.6	400			24.5	21.5^c	47
7	ZrO_2	Methyl stearate		400		94	30^d	12^d	77
8	Sn–Ce–Rh–O	Rape oil in methanol^d		385		96	50^e	14^e	78
9	ZrO_2	Acetic acid diluted in N_2	4^e	300	0.2 g	73	99^f		43

^{a} Concentration% in liquid product, ketone yield is a total of C_{31} and C_{35} ketones. ^{b} Selectivity. ^{c} Total diesel range alkane + alkene. ^{d} C_{35} ketone and C_{11}–C_{20} hydrocarbons (diesel range). ^{e} Rape oil: (C18 ME ~ 87%, C16 ME ~ 7%); yield: C_{35} ketone (47%), C_{31} ketone (3%) and hydrocarbons (14%). ^{f} 3.35 kPa HOAc in 20 mL min^{-1} N_2, 4 h time on stream.

acids reaction studies which repeats the uncertainty of the influence of surface area and porosity towards ketonization reaction.[10,50,71]

Along with desired palmitone, significant amount of pentadecane was also produced as a by-product *via* decarboxylation of palmitic acid (eqn (4)). However, pentadecane yield was found to be varied respective to added dopants on ZrO_2 catalyst. As aforementioned, changes in the physicochemical properties of catalysts have shown greater influence on specific reaction mechanisms such as decarboxylation route along with ketonization. Table 2 summarized the overall pentadecane yield that was observed from the catalytic reaction. On average 10–15% of pentadecane yield is produced as a part of palmitic acid ketonization reaction product. However, NiO/ZrO_2 exhibit significantly high pentadecane yield (24.9%) and suggest the decarboxylation route predominantly occurs under this catalyst system compared to ketonization reaction. Furthermore, its lowest palmitone yield (3.7%) also in agreement with the assumption whereby the presence of NiO on ZrO_2 is in favour of decarboxylation of palmitic acid. The presence of nickel was reported to selectively promote decarboxylation route that does not require hydrogen for the fatty acid deoxygenation reaction which produce series of paraffinic compounds.[48,72,73] Hence, the absence external hydrogen in our catalytic reaction proves that pentadecane production from palmitic acid occurred *via* decarboxylation through removal of CO_2. Furthermore, decarboxylation of oleic acid under similar condition using basic support catalyst without any metallic phase shows oxygen removal capacity in the form of CO_2 and produced *n*-heptadecane as a major product.[74]

Additionally, small amounts of C_{14} alkene, C_{17} ketones (methyl ketones) and other lighter hydrocarbons are also observed in the reaction product as a result of palmitone (C_{31} ketone) decomposition through either McLafferty Arrangement or the Norrish Type II cracking. These types of secondary degradations are profound in long chain fatty acids due the presence of electron donating alkyl groups in the γ-position that facilitate the cracking of products formed from ketonization.[75] Furthermore, intermolecular abstraction of γ-hydrogen by carbonyl group of the formed fatty ketone produce free radical intermediates that lead to molecular cleavage and reduce overall product selectivity.[47] This phenomenon explains the moderate palmitone yield of this investigation using modified

Fig. 4 Proposed reaction pathway for palmitic acid conversion over ZrO_2 supported metal oxides.

ZrO_2 based catalyst for palmitic acid ketonization reaction. The significant yield of by-product such as pentadecane is also appeared to be derived from palmitone cracking under the reaction condition. Therefore, based on the catalytic results a possible reaction pathways of palmitic acid ketonization is shown in Fig. 4. The carbon coupling of two palmitic acid molecule is proceeded *via* the ketonization reaction (Fig. 4(A)) whereby formation of the desired palmitone occurs with ejection of CO_2 and H_2O. Sequentially, palmitone also tend to undergo secondary degradation *via* β cleavage, producing C_{17} ketone and its C_{14} terminal alkene (Fig. 4(B)). Apart from this, direct deoxygenation of palmitic acid to pentadecane and pentadecene also occurs *via* decarboxylation route through elimination CO_2 (Fig. 4(C)) and CO by decarbonylation reaction (Fig. 4(D)). Additionally, cracking at other positions leads to other products like lighter alkanes ($<C_{14}$), alkenes as well as heavier ketones ($>C_{17}$ ketones) (Fig. 4(E)).

3.3 Effect of reaction parameters on ketonization reaction

Based on the catalytic screening, MnO_2 doped ZrO_2 appeared to be the most promising catalyst for neat palmitic acid conversion with highest palmitone yield of 27.7% under designated ketonization reaction conditions. However, reaction parameters such as temperature, retention time and catalyst loading play crucial roles in reaction efficiency and in attaining higher desired product yield.[10,11] The optimization of reaction parameters of MnO_2/ZrO_2 added palmitic acid ketonization reaction are summarized in Table 4. Firstly, palmitic acid conversion shows drastic improvements from 66.7% to 92.3% when the retention time of ketonization reaction raised from 1 to 3 h while further increment does not exhibit substantial progress. It appears to be 3 h retention time is enough to achieve optimal conversion rate with 27.7% of palmitone yield and started to show gradual decreasing trend beyond 3 h. This is due to the degradation of palmitone into various by-products at prolonged retention time which correlates with slight pentadecane yield increment.

The distinctive impact of reaction temperature is clearly visible in the overall reaction performance. At 3 h retention time, palmitic acid conversion shows a drastic decline after the reaction temperature reduced from 340 °C to 280 °C. This is due to the endothermic nature of the ketonization reaction that shows highest palmitic acid conversion of 92.4% at 340 °C and steadily dropped conversion of 13% at 280 °C. In addition, the major product composition of both palmitone and pentadecane shows the lowest yield in the range of 6–8% and 5–8% respectively in this investigation. This observation highlights the critical role of temperature in ketonization reaction to enhance overall yield and product selectivity. However, higher reaction temperatures are also reported to accelerate the product degradation due to the thermal instability of formed ketones that decrease the desired product yield.[79,80] Furthermore, Lu *et al.* (2018) recorded a sharp diminution in the pentanone selectivity after increasing the reaction temperature above 400 °C. Hence, an optimum reaction temperature is vital to maximise the ketone yield. However, due to reactor limitation
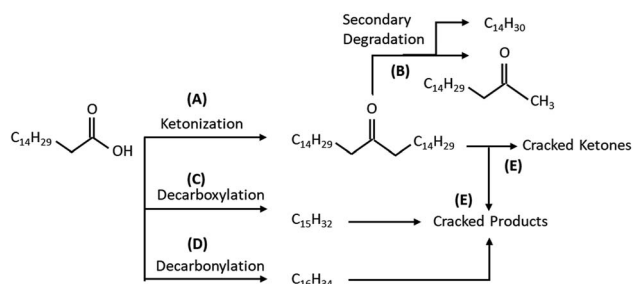
Table 4 Effect of reaction time, temperature and catalyst loading on palmitic acid conversion, palmitone and pentadecane yield

	Reaction time (h)	Reaction temperature (°C)	Catalyst loading (wt%)	$C_{15}COOH$ conversion (%)	Palmitone yield (mol%)	Pentadecane yield (mol%)
1	1		5	66.7	26.1	3.3
2	3			92.3	27.7	10.8
3	6	340		91.7	20.7	12.0
4	9			92.4	17.7	11.9
5	3	280	5	13.0	6.3	5.1
6		310		21.5	7.6	7.5
7		340		92.3	27.7	10.8
8	3	340	5	92.3	27.7	12.0
9			10	87.7	28.1	7.5
10			15	91.9	30.9	10.5

we only studied reaction temperature up to 340 °C and the ascending trend of palmitone yield agreed with literatures.

Lastly, after the identification of suitable reaction time (3 h) and temperature (340 °C) we proceeded with catalyst loading optimisation in the range of 5–15%. From both palmitic acid conversion and overall product yield it can be rationalised that there are no major changes observed with increasing catalyst loading from 5 to 15%. The negligible variation of feedstock conversion in the range of 87.7–92.3% shown by increasing MnO_2/ZrO_2 loading doesn't adlib the catalytic activity. Besides, only minor improvement in palmitone (~3.2%) and pentadecane yield (5.5%) occurred with 2- and 3-fold increase in catalyst loading. Therefore, 5% of catalyst is regarded as an adequate loading for palmitic acid ketonization to achieve optimum catalytic activity and product output.

Aside from this, FESEM-EDX analysis on the spent catalyst of MnO_2/ZrO_2 (Fig. 4S(A)†) reveals that there are no significant morphological differences among the spent and fresh catalyst. Additionally, the presence of Mn on the used catalyst was confirmed using EDX analysis and the dispersion was observed *via* elemental mapping which shows Mn remains well dispersed on the surface of ZrO_2 after the reaction. Based on the comprehensive parameters screening, we conclude that reaction condition of 3 h, and 340 °C with 5% catalyst loading is optimum for palmitic acid conversion to palmitone (27.7%) *via* ketonization reaction at our experimental set up. Even though, only moderate palmitone yield (27.7%) is observed, yet the application of undiluted, neat palmitic acid as a feedstock for ketonization remains a unique feature of this investigation. Furthermore, most of the fatty acid ketonization is carried out using short chained fatty acid or with solvents to dilute the feedstock to achieve high conversion and ketone yield. Apart from catalyst screening, the potential of direct neat fatty acid application in ketonization also explored in detail.

4. Conclusion

A series of modified ZrO_2 based catalyst are developed and used for catalytic conversion of palmitic acid *via* ketonization reaction. Among the developed catalyst, MnO_2/ZrO_2 exhibit the highest catalytic activity due to the presence of intermediate

acid and basic sites on the catalyst surface. This unique catalyst surface nature allows the moderate strength absorption of palmitic acid which transform into palmitone or pentadecane and detached easily from the active sites. Therefore, under the optimized reaction condition of 3 h, 340 °C and 5% of catalyst loading, highest conversion of 92.3% is achieve with obtained palmitone and pentadecane yield of 27.7% and 10.8% respectively. Among the reaction parameters, temperature and time was found to be the most vital aspect of ketonization reaction that significantly influence the overall catalytic activity. Besides, the moderate product yield of this investigation is mainly due to the application of undiluted fatty acid in ketonization reaction which requires detailed studies to enhance the product selectivity near future.

Conflicts of interest

There are no conflicts to declare.

Acknowledgements

References

1 J. G. Immer, M. J. Kelly and H. H. Lamb, *Appl. Catal., A*, 2010, **375**, 134–139.
2 N. Aranda-pérez, M. P. Ruiz, J. Echave and J. Faria, *Appl. Catal., A*, 2017, **531**, 106–118.
3 *Malaysian Palm Oil Industry*, http://www.mpoc.org.my/Malaysian_Palm_Oil_Industry.aspx.
4 Neste, *Palm fatty acid distillate (PFAD) – a residue from palm oil refining process*, https://www.neste.com/corporate-info/sustainability/sustainable-supply-chain/pfad-residue-palm-oil-refining-process.
5 B. Tay, Y. Ping and M. Yusof, *Oil Palm Bull.*, 2009, **59**, 5–11.
6 C. A. Gaertner, J. C. Serrano-Ruiz, D. J. Braden and J. A. Dumesic, *Ind. Eng. Chem. Res.*, 2010, **49**, 6027–6033.

7 S. Wang and E. Iglesia, *J. Catal.*, 2017, **345**, 183–206.

8 M. Renz, *Eur. J. Org. Chem.*, 2005, 979–988.

9 R. Kumar, N. Enjamuri, S. Shah and A. S. Al-fatesh, *Catal. Today*, 2018, **302**, 16–49.

10 G. Zalewski, E. Burno and A. Jerzak, *Appl. Catal., A*, 2014, **470**, 278–284.

11 I. L. Simakova and D. Yu, *J. Energy Chem.*, 2016, **25**, 208–224.

12 F. Fally, V. Perrichon, H. Vidal, J. Kaspar, G. Blanco, J. M. Pintado, S. Bernal, G. Colon, M. Daturi and J. C. Lavalley, *Catal. Today*, 2000, **59**, 373–386.

13 T. N. Pham, T. Sooknoi, S. P. Crossley and D. E. Resasco, *ACS Catal.*, 2013, **3**, 2456–2473.

14 D. Li, F. Yao and Q. X. Guo, *Energy Fuels*, 2009, **23**, 564–568.

15 T. K. Phung, A. A. Casazza, P. Perego, P. Capranica and G. Busca, *Fuel Process. Technol.*, 2015, **140**, 119–124.

16 A. S. Hussain, S. M. Aleem and M. R. Ramli, *Development of low viscosity base oil*, 2019.

17 G. Baskar and S. Soumiya, *Renewable Energy*, 2016, **98**, 101–107.

18 P. Massa, F. Ivorra, P. Haure and R. Fenoglio, *J. Hazard. Mater.*, 2011, **190**, 1068–1073.

19 Y. Zhang, Q. Cheng, Y. Zhang, G. Song and C. Zhou, *J. Taiwan Inst. Chem. Eng.*, 2020, **109**, 103–110.

20 J. C. Russ, *Adv. X-Ray Anal.*, 1985, **28**, 11–16.

21 N. Pal and A. Bhaumik, *RSC Adv.*, 2015, **5**, 24363–24391.

22 T. Aysu and A. Sanna, *Bioresour. Technol.*, 2015, **194**, 108–116.

23 S. W. Banks and A. V. Bridgwater, *Catalytic fast pyrolysis for improved liquid quality*, Elsevier Ltd, 2016.

24 C. Bueno-Ferrer, S. Parres-Esclapez, D. Lozano-Castelló and A. Bueno-López, *J. Rare Earths*, 2010, **28**, 647–653.

25 S. D. Davidson, K. A. Spies, D. Mei, L. Kovarik, I. Kutnyakov, X. S. Li, V. Lebarbier Dagle, K. O. Albrecht and R. A. Dagle, *ACS Sustainable Chem. Eng.*, 2017, **5**, 9136–9149.

26 W. N. N. Wan Omar and N. A. S. Amin, *Fuel Process. Technol.*, 2011, **92**, 2397–2405.

27 D. R. Burri, K. M. Choi, S. C. Han, A. Burri and S. E. Park, *Bull. Korean Chem. Soc.*, 2007, **28**, 53–58.

28 E. K. C. Pradeep, T. Habu, H. Tooriyama, M. Ohtani and K. Kobiro, *J. Supercrit. Fluids*, 2015, **97**, 217–223.

29 Z. Hossain, M. B. I. Chowdhury, A. K. Jhawar, W. Z. Xu and P. A. Charpentier, *Fuel*, 2018, **212**, 470–478.

30 Z. Wen, X. Yu, S. Tu, J. Yan and E. Dahlquist, *Appl. Energy*, 2010, **87**, 743–748.

31 A. Islam, Y. H. Taufiq-Yap, C. M. Chu, P. Ravindra and E. S. Chan, *Renewable Energy*, 2013, **59**, 23–29.

32 Z. Zhang, L. Zhang, M. J. Hülsey and N. Yan, *Mol. Catal.*, 2019, **475**, 110461.

33 B. Bachiller-Baeza, I. Rodriguez-Ramos and A. Guerrero-Ruiz, *Langmuir*, 1998, **14**, 3556–3564.

34 K. Yoshikawa, H. Sato, M. Kaneeda and J. N. Kondo, *J. CO$_2$ Util.*, 2014, **8**, 34–38.

35 N. Asikin-Mijan, H. V. Lee, Y. H. Taufiq-Yap, G. Abdulkrem-Alsultan, M. S. Mastuli and H. C. Ong, *Energy Convers. Manage.*, 2017, **141**, 325–338.

36 V. R. Choudhary and V. H. Rane, *J. Catal.*, 1991, **422**, 411–422.

37 M. Haneda, K. Takamura, Y. Doi, N. Bion and L. Vivier, *J. Mater. Sci.*, 2017, **52**, 5835–5845.

38 P. Kumar, P. With, V. C. Srivastava, K. Shukla and I. M. Mishra, *RSC Adv.*, 2016, 110235–110246.

39 M. Glorius, M. A. C. Markovits and C. Breitkopf, *Catalysts*, 2018, **8**, 1–25.

40 K. Świrk, Y. Wang, C. Hu, L. Li, P. Da Costa and G. Delahay, *Catalysts*, 2021, **11**, 1–15.

41 S. E. Kondawar, R. B. Mane, A. Vasishta, S. B. More, S. D. Dhengale and C. V. Rode, *Appl. Petrochem. Res.*, 2017, **7**, 41–53.

42 K. Tanabe, *Mater. Chem. Phys.*, 1985, **13**, 347–364.

43 S. T. Almutairi, E. F. Kozhevnikova and I. V. Kozhevnikov, *Appl. Catal., A*, 2018, **565**, 135–145.

44 Y. A. Zaytseva, V. N. Panchenko, M. N. Simonov, A. A. Shutilov, G. A. Zenkovets, M. Renz, I. L. Simakova and V. N. Parmon, *Top. Catal.*, 2013, **56**, 846–855.

45 E. Heracleous, D. Gu, F. Schüth, J. A. Bennett, M. A. Isaacs, A. F. Lee, K. Wilson and A. A. Lappas, *Biomass Convers. Biorefin.*, 2017, **7**, 319–329.

46 T. Kulik, B. Palianytsia and M. Larsson, *Catalysts*, 2020, **10**, 179.

47 T. Maluangnont, C. Dararat, T. Kulrat, S. Soontontaweesub, T. Anothaiwalaikul, P. Bunprechawong, R. Chanda, J. Kanchanawarin, P. Kidkhunthod and T. Sooknoi, *Catal. Commun.*, 2017, **102**, 123–126.

48 C. Miao, O. Marin-Flores, S. D. Davidson, T. Li, T. Dong, D. Gao, Y. Wang, M. Garcia-Pérez and S. Chen, *Fuel*, 2016, **166**, 302–308.

49 X. Yih, W. Gao, H. Chyuan, H. Voon, J. Ching, W. Hsin and K. Teong, *Renewable Sustainable Energy Rev.*, 2019, **112**, 834–852.

50 O. Nagashima, S. Sato, R. Takahashi and T. Sodesawa, *J. Mol. Catal. A: Chem.*, 2005, **227**, 231–239.

51 M. Glinski, *Appl. Catal., A*, 1995, **128**, 209–217.

52 J. Jia, R. Ran, R. Guo, X. Wu and D. Weng, *Prog. Nat. Sci.: Mater. Int.*, 2018, **28**, 296–300.

53 J. F. Moulder, W. F. Stickle, P. E. Sobol and J. Chastain, *Handbook of X-ray Photoelectron Spectroscopy*, Perkin-Elmer Corporation, 1992.

54 M. Oku, K. Hirokawa and S. Ikeda, *J. Electron Spectrosc. Relat. Phenom.*, 1975, **7**, 465–473.

55 B. Smith, L. Li, D. D. Perera-Solis, L. F. Gildea, V. L. Zholobenko, P. W. Dyer and H. C. Greenwell, *Inorganics*, 2018, **6**(4), 121.

56 R. Klimkiewicz, H. Grabowska and L. Syper, *Pol. J. Environ. Stud.*, 2000, **9**, 179–181.

57 M. S. M. Al-Ghamdi and H. Bayahia, *Mediterr. J. Chem.*, 2017, **6**, 1–6.

58 R. W. Snell and B. H. Shanks, *Appl. Catal., A*, 2013, **451**, 86–93.

59 G. Ruderman, E. R. Caffarena, I. G. Mogilner and E. J. Tolosa, *J. Solution Chem.*, 1998, **27**, 935–948.

60 Y. Yamada, M. Segawa, F. Sato, T. Kojima and S. Sato, *J. Mol. Catal. A: Chem.*, 2011, **346**, 79–86.

61 H. Bayahia, *Sci. J. Chem.*, 2018, **6**, 11.

62 Y. Lee, J. W. Choi, D. J. Suh, J. M. Ha and C. H. Lee, *Appl. Catal., A*, 2015, **506**, 288–293.

63 J. A. Lopez-Ruiz, A. R. Cooper, G. Li and K. O. Albrecht, *ACS Catal.*, 2017, **7**, 6400–6412.

64 F. Lu, B. Jiang, J. Wang, Z. Huang, Z. Liao, Y. Yang and J. Zheng, *RSC Adv.*, 2017, **7**, 22017–22026.

65 Q. Yu, Y. Guo, X. Wu, Z. Yang, H. Wang, Q. Ge and X. Zhu, *ACS Sustainable Chem. Eng.*, 2021, **9**, 7982–7992.

66 S. Ding, H. Wang, J. Han, X. Zhu and Q. Ge, *Ind. Eng. Chem. Res.*, 2018, **57**, 17086–17096.

67 B. Boekaerts and B. F. Sels, *Appl. Catal., B*, 2021, **283**, 119607.

68 S. Ding, J. Zhao and Q. Yu, *Catalysts*, 2019, **9**, 17–22.

69 H. Ling, Z. Wang, L. Wang, C. Stampfl, D. Wang, J. Chen and J. Huang, *Catal. Today*, 2020, **351**, 58–67.

70 H. Jahangiri, A. Osatiashtiani, J. A. Bennett, M. A. Isaacs, S. Gu, A. F. Lee and K. Wilson, *Catal. Sci. Technol.*, 2018, **8**, 1134–1141.

71 R. W. Snell and B. H. Shanks, *ACS Catal.*, 2014, **4**, 512–518.

72 Y. Cao, Y. Shi, J. Liang, Y. Wu, S. Huang and J. Wang, *Chem. Eng. Sci.*, 2017, **158**, 188–195.

73 B. Peng, C. Zhao, S. Kasakov, S. Foraita and J. A. Lercher, *Chem.–Eur. J.*, 2013, **19**, 4732–4741.

74 J. Na, B. E. Yi, J. N. Kim, K. B. Yi, S. Park, J. Park, J. Kim and C. H. Ko, *Catal. Today*, 2010, **156**, 44–48.

75 K. Lee, M. Y. Kim and M. Choi, *ACS Sustainable Chem. Eng.*, 2018, **6**, 13035–13044.

76 T. K. Phung, A. A. Casazza, B. Aliakbarian, E. Finocchio, P. Perego and G. Busca, *Chem. Eng. J.*, 2013, **215–216**, 838–848.

77 B. Oliver-Tomas, M. Renz and A. Corma, *Ind. Eng. Chem. Res.*, 2017, **56**, 12870–12877.

78 R. Klimkiewicz, H. Teterycz, H. Grabowska, I. Morawski, L. Syper and B. W. Licznerski, *J. Am. Oil Chem. Soc.*, 2001, **78**, 533–535.

79 R. Klimkiewicz, E. Fabisz, I. Morawski, H. Grabowska and L. Syper, *J. Chem. Technol. Biotechnol.*, 2001, **76**, 35–38.

80 M. Lu, A. W. Lepore, J. Choi, Z. Li, Z. Wu, F. Polo-garzon and M. Z. Hu, *Catalysts*, 2018, **8**, 643.